Ionic liquids under nanoscale confinement

Francesca Borghi & Alessandro Podestà

Published online: 03 Apr 2020.

Submit your article to this journal ⬘

View related articles ⬘

View Crossmark data ⬘

Taylor & Francis
Taylor & Francis Group

Ionic liquids under nanoscale confinement

Francesca Borghi [ID] and Alessandro Podestà [ID]

CIMaINa and Dipartimento di Fisica "Aldo Pontremoli", Università degli Studi di Milano, Milano, Italy

ABSTRACT

The confinement of room-temperature ionic liquids (ILs) in nanoscale geometries, where at least one, but often all three dimensions are reduced down to lengths comparable to the anion-cation size, put the ILs into a quite different condition with respect to their bulk phase. An understanding of the properties of the ILs confined in a nanoscale-constrained geometry is of both fundamental and practical interest. In particular, the spatial restriction of ILs promotes a strong interaction of the ILs with the surface of the confining matrix, which strongly affects their properties, like the phase transition behavior, layering near surface walls, wetting, as well as ionic mobility. This short review is especially concerned with the interfacial confinement of ILs on solid substrates, in the form of very thin films, or inside porous nanomaterials.
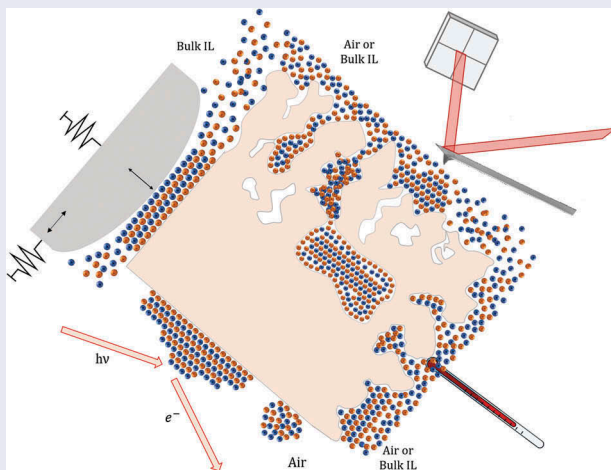
1. Introduction

Room-temperature ionic liquids (RTILs or simply ILs) are salts, which are typically liquid at temperatures well below 100°C [1,2]. ILs possess several interesting properties, among many others negligible vapor pressure and

CONTACT Alessandro Podestà ✉ alessandro.podesta@mi.infn.it CIMaINa and Dipartimento di Fisica "Aldo Pontremoli", Università degli Studi di Milano, via Celoria 16, Milano 20133, Italy

controlled miscibility, non-flammability, good thermal stability, and wide electrochemical window. The virtually unlimited versatility in designing the cation-anion pair allows to produce ILs with tailored physicochemical properties to support a large number of applications: ILs are employed as electrolytes in photoelectrochemical and energy storage devices [3], as advanced lubricants in tribology [4–7], as reaction media in synthesis and catalysis [1,2], as well as solvents in the chemical industry [8].

In many applications, ILs interact with solid surfaces, either because they are employed as electrolytes [9] or because they are used as thin lubricant layers [6]. In all these cases, the most relevant processes determining the performance of the devices take place at the liquid/solid interface, in conditions of strong spatial confinement [10], either because the lubricant IL film is only a few nanometers thick or because the surface of the solid electrode is rough and porous at the nanoscale, as in the case of electrochemical supercapacitors [11–13], solar cells [14,15], and batteries [15–17].

The use of ILs into nanoporous matrices leads to advanced materials, called ionogels, which integrate the peculiar properties of ILs into soft polymers and robust porous organic/inorganic materials [18–20]. Ionic liquids also prevent the solid network/matrix from collapsing into a compact mass, while the network confines the ionic liquid and prevents it from flowing away.

Since the early studies on ionic liquids confined into porous silica gels conducted by Dai et al. [21], ionogels have been deeply experimentally and theoretically investigated in many disciplines and for different advanced applications, such as energy storage devices (electrochemical batteries, fuel cells, supercapacitors) [22–24], drug delivery systems [25], as well as in organic synthesis, heterogeneous catalysis and gas separation [26–28].

The confinement of ILs in nanoscale geometries, where at least one dimension is reduced down to lengths comparable to the ion size, put the IL in a quite different condition with respect to the bulk phase, whether they are dispersed into a polymeric host or entrapped into a porous stiff matrix. An understanding of the properties of the ILs confined in a nanoscale-constrained geometry is of both fundamental and practical interest. In particular, the spatial restriction and low dimensionality promote a strong interaction of the ILs with the walls of the confining matrix, resulting in physicochemical behavior of the confined ILs, in terms of phase transition behavior [29–31], wetting [32], layering near surface walls [33,34], as well as mobility [35–37], much different from the corresponding bulk properties.

We emphasize here that confinement of ILs can be found not only in three-dimensional porous matrices, due to the presence of constraining surrounding walls in the pores, but also in more open geometries. In these cases, the constraining walls are present only along one or two directions, either in a static configuration or dynamically removed during the operation of the device. In general, confinement takes place whenever the interaction

of the IL with the constraining surface(s) becomes relevant with respect to the mutual interaction of IL ions, i.e. when the ratio of the wall surface and the volume available to the IL become large.

Figure 1 exemplifies this point showing the relevant interfaces and confining conditions that we will consider in this review.

The first case (Figure 1(a)) represents a spatial confinement induced by the presence of a counter surface. For instance, in tribological interfaces, a slider that is displaced relatively to the surface under study represents the counter surface. This condition can be reproduced in the laboratories by bringing a suitable probe (either an atomic force microscopy, AFM, tip [33], or the mica cylinders of a surface force apparatus, SFA [10]), in contact with the surface, by both approaching-retracting the probe vertically, in and out of contact, and sliding it horizontally across the other surface.

Confinement can be also induced when a tiny amount of IL is deposited onto a compact (i.e. nonporous) solid surface, in the sub-monolayer and in the thin film regime, so to obtain a partial coverage of the substrate (Figure 1(b)) [38–40]. No IL in the bulk liquid phase is present above the substrate, at odd with the case of Figure 1(a). In this case, the nanoscale confinement is along the vertical direction, even though there is no upper constraining wall, and the confinement length is far larger than the typical ion pair size.
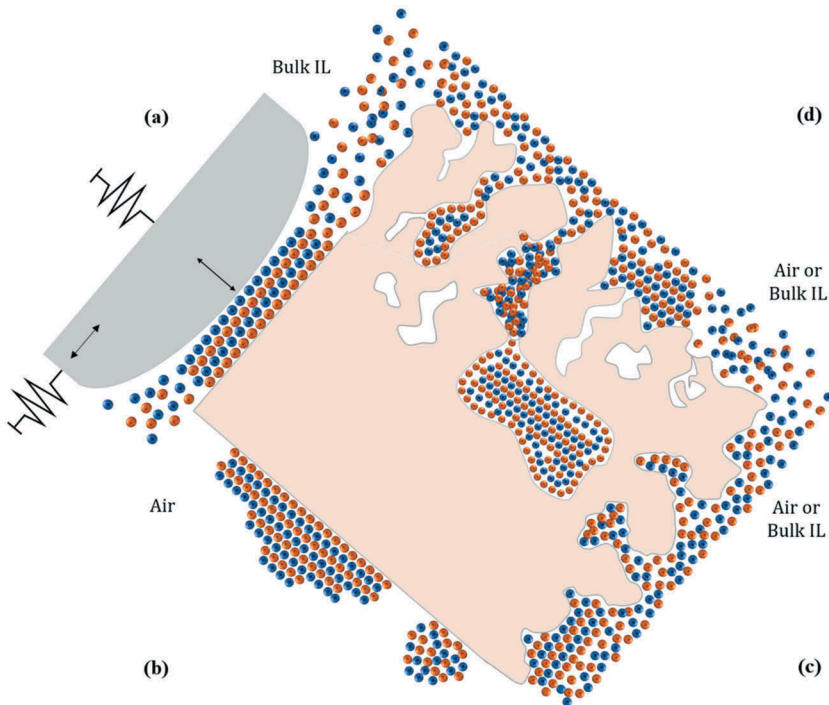

Figure 1. Ionic liquids in different nanoscale-confined geometries.

Nanoscale surface roughness on compact solid surfaces produces a distribution of open surface pores with varying width, volume and aspect ratio, depending on the peculiar surface morphology, whose walls can offer confinement conditions for the IL at the very interface, also in the presence of a bulk amount of IL in the liquid phase above that interface (Figure 1(c)).

Eventually, the more complex, yet more representative, case is depicted in Figure 1(d), where the solid substrate (typically the electrode material on a device) is nanoporous. In this case, besides the interfacial confinement provided by the open pores due to surface roughness, also confinement in the bulk materials, in pores that can be as small as the ion pair size, takes place. The open surface pores are typically connected to the network of internal pores.

Depending on the nature of the host matrix several cases are possible, from disordered, nanostructured solid matrices, to ordered nano and mesoporous structures, passing through porous nanocomposite materials where pores are provided by the molecular structure of the components (as in the case of carbon nanotube – based materials).

This short review is concerned with the interfacial confinement of ILs into very thin films or in porous nanomaterials, and with the experimental characterization of the changes of their physicochemical properties.

First, we will present some examples of ionogels typically employed in advanced applications, where the IL is confined into nanoporous matrices, emphasizing ionogels whose solid nanoporous matrix is produced by means of cluster-assembling from the gas phase [41]. These materials possess a peculiar nanostructure and porosity with respect to both nanocomposites assembled using ordered carbon nanotubes or other porous carbon materials or those based on silica nanoparticles. We will then discuss some experimental observations of how the nanoscale confinement affects the physical properties of the nanoconfined ILs.

We will focus in particular on the cases depicted in Figure 1(b–d), when ILs find suitable confinement conditions in the form of thin films deposited on solid supports, either smooth or rough at the nanoscale; either compact or nanostructured and nanoporous.

The results discussed in this review can be of direct interest for applications in different fields, like in energy storage/conversion devices employing ionogels formed by nanoporous matrices impregnated by IL electrolytes, but also for ILs – lubricated or ILs-assisted catalytic interfaces. On the other hand, the confining matrices here described represent versatile platforms for experimentally assessing fundamental aspects of the physics of ILs under nanoscale confinement.

2. Nanostructured, nanoporous ionogels

Ionogels consist in a solid host matrix (either inorganic or organic) entrapping the ionic liquid and can be viewed as hybrid materials, where the properties of the host and those of the impregnating IL are combined.

The choice of the structural properties of the porous host is very important for the successful confinement of ILs, as well as their potential applications, because the structure and the properties of confined ILs are significantly influenced by the pore structure and the surface chemistry of the hosts, which determines the nature and extent of the IL-pore wall interactions. In ionogels, the common solid porous hosts for ILs are nanoporous carbons [35] as well as nanoporous silica [22,36,42–44] and metal-organic frameworks (MOFs) [45,46]. Comprehensive descriptions of ionogels can be found in Refs [20,42].

Different forms of nanostructured porous carbon in particular are used in applications for energy storage like the electrical double-layer capacitors (EDLCs) [47,48]. ILs are here employed as more efficient electrolytes compared to the conventional ones based on water [49], owing to their wide electrochemical window and high ion density, as well as good thermal stability and non-volatility [22,44,50–52].

Recently, cluster-assembled nanostructured carbon (ns-C) films produced by supersonic cluster beam (SCBD) deposition [41,53] with high porosity and specific surface area [54] have been combined with ILs for the production of planar micro EDLCs [13,55], schematically shown in Figure 2. Ns-C allowed the penetration of IL ions and their reversible adsorption and organization into an electrostatic double layer in the ns-C porous matrix over a wide range of electrode thicknesses [12].
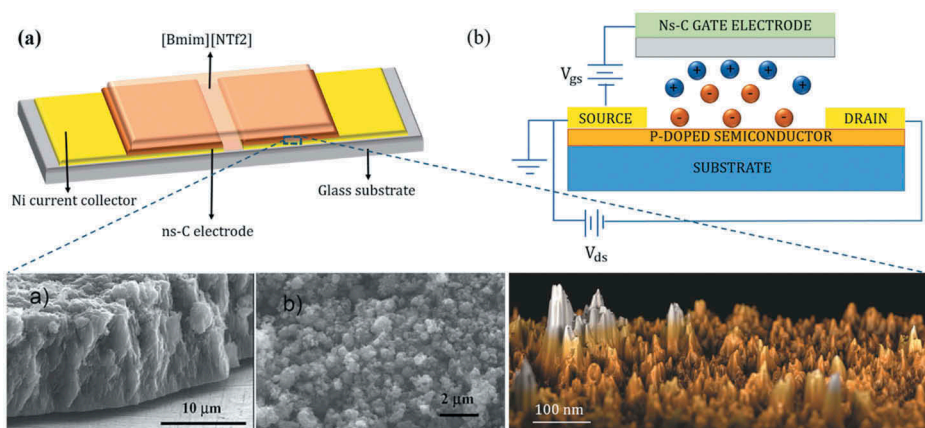
Figure 2. (a) Schematic representation of a planar ns-C-based supercapacitor, as described in Ref [13], and (b) of an electrolyte-gated transistor, as described in Refs [55,61]. SEM and AFM images show, at different magnification, the granular and rough morphology of the porous bulk and upper surface of ns-C film. Partially adapted with permission from Ref [60].

Films produced by SCBD are good platforms to study the influence of the nanostructure of the host materials on the properties of ILs. In thin films produced by SCBD, nanometer-sized clusters form a disordered porous matrix characterized by features extending from the nano to the mesoscopic scale [56,57] [Bettini et al., Springer Handbook of Surface Science, in press]; the porosity (void fraction) of these films is typically between 60% and 80% [54]. The external interface of these films is rough; morphological features with lateral dimensions ranging from the size of the primeval incident clusters to hundreds of nanometers, or microns, depending on the film thickness, are organized in a disordered, statistically scale-invariant (self-affine) morphology [56], with the characteristic surface parameters (like the root-mean-square roughness) scaling according to simple power laws [41,56,58]. At the rough outer interface, open pores with locally high-aspect-ratio and nanometer-scale dimensions [56,58,59] can accommodate the ionic liquid, which can also impregnate the bulk nanostructured film; high spatial confinement can therefore occur, both inside the bulk of the microporous matrix and on the mesoporous open interface.

Ns-C electrodes have been used also as gate electrodes inside hybrid flexible transistors (electrolyte-gated transistor) [55,61], based on organic polymer and ionic liquid as electrolyte (also schematically shown in Figure 2(b)).

Designing and optimizing the properties of the ionogels requires a better understanding of the effects of the geometrical confinement on the properties of the ILs.

3. The effect of confinement on the structural properties of ionic liquids

The interactions taking place at the interface between a liquid and a solid matrix result in physical and chemical behavior of the confined liquid, which can be very different from the ones characterizing the liquid in the bulk. Different phase transition behavior, wetting, layering near surface walls, shift in glass transition, melting and freezing points have been reported for ILs in confined geometries [18,20,31,32,62,63].

The microenvironment of a liquid confined in small pores is markedly different from that of the bulk liquid. In the vicinity of a solid surface, a liquid molecule has fewer neighbors. In the case of ILs, which are composed of bulky charged species, this may have an influence on the interactions among these species in the vicinity of the pore wall. If the pore is small enough, comparable in size to the ionic dimensions, interfacial interactions become predominant and the bulk properties can be lost.

There is increasing evidence that extreme confinement of ILs can lead to a change of the freezing-melting temperature. The change in the melting point of a liquid in a confined geometry is described by the Gibbs–Thomson equation

[64], which usually accounts for the depression of the freezing – melting point of the liquid (as in the case of water [65]) into a pore. This equation predicts a reduction of the freezing-melting temperature inversely proportional to the pore dimension and proportional to the difference $\Delta\gamma=\gamma_{wl}-\gamma_{ws}$ between the wall-liquid surface energy γ_{wl} and the wall-solidified liquid surface energy γ_{ws}. The degree of freezing induced by confinement therefore strongly depends on the pore size and IL-pore wall interaction.

In the specific case of the ILs (and also other liquids, as reported for cyclohexane in Ref [66]), the surface energy difference can change sign, and the freezing temperature can be higher, leading to solidification of the IL inside the pores at room temperature. The increase of the melting temperature was inferred by force measurements on ILs squeezed between either insulating and metallic surfaces [31,67] or spontaneously intercalated between mica sheets upon drop-casting deposition [68]; direct differential scanning calorimetry measurements revealed this effect for ILs inside multi-walled carbon nanotubes [29] and into ordered mesoporous silica [69].

Other authors however obtained opposite results consistent with the classical (and in some case marked) depression of the melting–freezing temperature, for the confinement of ILs in both nanoporous silica [63] and metallic silver [70] matrices, as well as metal–organic frameworks (MOFs) [71]. Moreover, recent conductivity measurements through glass nanochannels did not reveal any significant reduction in the ionic mobility that could be attributed to confined-induced freezing of the IL [72]. Table 1 reports a summary of the most relevant properties of the confined ILs discussed in the cited works.

In some cases, the observed melting–freezing transition in nanoconfined geometries spans a relatively broad range of temperatures, which can be attributed to a broad distribution of molecular environments of the confined IL. The IL thus forms an amorphous phase inside the pores, rather than a crystalline one, as in the case reported in Ref [73].

The density and the ionic mobility of nanoconfined ILs are the target of several studies, including numerical simulations. These studies can reveal layering of the IL in confined geometries, although this phenomenon is not necessarily associated with a liquid to solid transition.

The authors of Ref [74] have estimated by numerical simulations the effect of confinement and surface chemistry on the density of the IL confined in amorphous silica pores. Despite the screening of the electrostatic interactions is very effective in ILs (the Debye length is of the order of the ionic dimensions), electrostatic interactions, both between the ions and the pore walls, and between ions and ions, are found to be predominant and to compete according to the surface to volume ratio of the pore. Strong layering in the pores is observed, extending from wall-to-wall across distances larger than the IL dimensions, although the density of the confined

Table 1. Summary of the confined IL properties discussed in this work and in the cited literature.

Ionic liquids	Confining matrices	Relevant properties of the confined ILs	Potential application field	Ref.
[Bmim][PF6]	Microporous carbon, pore sizes between 0.3 and 1.7 nm	Ions approach the surface more closely than in the planar electrode → larger charge stored inside microporous electrodes	EDLCs	[24]
[Bmim][PF6]	Ordered mesoporous silica (MCM-41 and SBA-15)	Confined IL fills the matrix pores. No evidence for ordering. Partial pore filling obtained for the chemically grafted samples, with a degree of ordering of the IL.	Supported ionic liquid phase systems (SILPS)	[28]
[Bmim][PF6]	Multiwalled carbon nanotubes (MWNTs)	Formation of polymorphous IL crystals, melting point above 200°C	Catalysts, gas capture sorbents	[29]
[Bmim][BF4],[Bmim][PF6], [Bmim][Tf2N]	Graphene multilayers	Melting point enhancement and crystallization of ILs	Catalysts, gas capture sorbents	[30]
[Bmim][BF4]	AFM tungsten tip on mica, HOPG, doped silicon, and platinum substrates	Solid-like IL phase below a threshold thickness, due to capillary freezing upon confinement. Wetting properties tuned by the electronic screening inside the confining substrates	Lubrication	[31]
[Bmim][PF6]	Mesoporous TiO$_2$ films	Enhanced adhesion of IL to the matrix and reduced contact angle	CO$_2$ capture and separation	[32]
EAN, PAN, C$_2$mimAc	Sharp Si$_3$N$_4$ tips (radius 20 nm) on mica, silica, graphite substrates	Solvation layers are formed depending on the surface charge and roughness	Lubrication	[33]
EAN, EtAN, EAF, PAF, EMAF, DMEAF	Sharp Si$_3$N$_4$ tips (radius 20 nm) on mica substrate	Solvation layers tuned by modifying the cation and anion molecular structure	Lubrication	[34]
[Bmim][Tf2N]	Mesoporous carbon matrix with cylindrical pores (8.8 ± 2.1 nm in diameter)	Enhanced rather than suppressed diffusivity of cations compared to the bulk liquid	Electrochemical devices	[35]
[Hmim][PF6]	Oxidized nanoporous silicon membranes; average pore diameter 7.5 ± 0.7 nm	Remarkable increase of the diffusion coefficient of the confined IL upon silanization of the membranes.	Power sources and energy storage devices	[36]
[Bmim][Tf2N]	Highly ordered (KIT-6) three-dimensional cubic mesopore silica structure	Reduction of the cation diffusivity by a factor of two compared to the bulk CO$_2$/IL mixture or the pure IL	CO$_2$ separation in mixtures of gases	[37]
[Bmim][PF6]	Mica surfaces	Multilayer structures, including liquid and solid phases of IL	Microelectromechanical systems (MEMS)	[38]
[Emim][Tf2N]	Glass substrate	Order in the first molecular layer	SILPS	[40]
[Emim][BF4]	Mesoporous MCM-41 silica ordered matrix	The glass transition temperature increased compared to the bulk IL	SILPS	[62]
[Bmim][CF3SO3], [Bmim][PF6], [Emim][PF6], [Bmim][(CF3SO2)2N]	Controlled-pore glasses, mean pore diameter from 7.5 to 50 nm	Melting point depression of ionic liquids confined in nanopores	SILPS	[63]

(Continued)

Table 1. (Continued).

Ionic liquids	Confining matrices	Relevant properties of the confined ILs	Potential application field	Ref.
[Hmim] [EtSO₄]	Mica vs mica surfaces, silica probe vs mica surface	Ordered structure that extends up to 60 nm from the surface. (importance of humidity)	Lubrication	[67,93]
[Bmim][NTf2]	Mica vs mica surfaces	IL crystals, up to several dozen layers. Melting temperature 73 K higher than that of the bulk IL.	Catalysts, gas capture sorbents	[68]
[Emim][FSI]	Ordered mesoporous silica MCM-41	IL compressed in the nanopores of the MCM-41 matrix; increased melting point	SILP	[69]
[Bmim][NO₃]	Silver matrix	Highee thermal stability; first-order transitions shifted toward lower temperatures.	Catalysis	[70]
[Emim][NTf2]	Metal-organic framework (ZIF-8)	No heat anomaly down to 123 K in the DSC measurements, differently from bulk IL (freezing and melting at 231 and 257 K)	Catalysis	[71]
[Emim][BF4], [Bmim][BF4], [Bmim][PF6]	Silica nanocapillaries	No long range freezing effects due to confinement in nanopores with diameters as low as 20 nm	Catalysis	[72]
[C₂Py][BTA]-d₁₀	Porous silica material	Amorphous phase over a temperature range of 30 K, at lower temperatures than in the bulk IL. Above this transition range, the IL shows liquid-like behavior.	Catalysis, SILPS	[73]
[Bmim][NTf2] (simulation)	Hydroxylated amorphous silica nanopores; pores width from 2.0 to 4.0 nm	Ionic conductivity of the confined IL is found to be similar to the bulk	Lubricants, drug delivery systems	[74]
[Emim][NTf2] (simulation)	Slit graphitic nanopore of width 5.2 nm	Ions inside the pore move slower than in the bulk IL; depending on the σ the parallel component of the MSD of the ions near the pore wall or in the center of the pore becomes comparable one of bulk ions	EDLCs	[75]
[Emim][NTf2] (simulation)	Rutile (110) slit nanopore of width H = 5.2 nm	The dynamics of the IL inside a slit rutile pore is significantly slower than inside a slit graphitic pore	EDLCs	[76]
[Bmim][PF₆] (simulation)	Radius-various H2 and slit-shaped H3 pores of the methylated silica	Confined IL molecules form a self-organized ordering only in H3 nanopores	Supercapacitors, fuel cells, drug deliveries	[77]
[Cmim][PF6] (simulation)	H2, H3 and H4 narrow slit-like nanopores	H2 and H4 nanopores destroy nanoscale segregation; confined IL form a more close packing in the H3 nanopores	Supercapacitors, fuel cells, drug deliveries	[78]
[Hmim][NTf2], [Hmim][CF₃SO₃], [Hmim][OAc]	Mesoporous silicas (silica gels, MCM-41, SBA-15)	On MCM-41 and SBA-15, homogeneous layers of ionic liquid are formed, if the ionic liquid is not too hydrophobic	Catalysis	[79]
[Hmim][TFS],	SiO₂ substrates (0.4–3.8 nm RMS) and rough silica colloidal tip (1–9 nm RMS)	Local ordering at the multi-asperity contacts	Energy storage/conversion devices	[81]

(Continued)

Table 1. (Continued).

Ionic liquids	Confining matrices	Relevant properties of the confined ILs	Potential application field	Ref.
[Emim][TFSA], [BMP][TFSA]	Au(111) and Si$_3$N$_4$ AFM tip	Multiple solvation layers; the force required to rupture the innermost solvation layer is greater for [BMP]TFSA than for [EMIm]TFSA, due to stronger cation surface interactions	Electrochemical devices	[83]
[(OH)C2C1im][BF4] (simulation)	Silica, alumina and borosilicate glass substrates	Orientation and stratification of IL ions	Tribology, heterogeneous catalysis	[84]
[N1114][C1SO3], [N1114][C4SO3], [N1124][C4SO3]	Smooth iron surface	First ordered layer of ions near the surface	Lubricants	[85]
[Bmim][NTf2] (experiments and simulations)	Mica, amorphous silica, and oxidized Si(110)	Terraced solid-like structures of mesoscopic area (1–100 μm^2) and 50 nm height, which behave like insulator layers with a relative dielectric constant significantly smaller than those measured in the bulk ionic liquid	Lubricants and MEMS, thin supported IL coatings	[39,86,88,89,94]
[Bmim][NTf2]	Nanostructured oxidized silicon thin film	Solid IL terraces, more than 100 nm high	Electrochemical devices	[87]
[Bmim][FAP]	Mica	Flat layers extending few nm	Lubrication, catalysis	[90]
[Bmim][TFSI]	HOPG, mica, rubrene (001) surface	Stable step-terrace structure and softer solvation layers of similar layer thickness on HOPG and mica; not on rubrene	EDL supercapacitors, OFETs	[91]
[Bmim][BF$_4$]	Platinum substrate; bias voltage applied	Micrometer-scale uniform films with a thickness of about 4 nm	Lubricants for MEMS/NEMS	[92]

IL, as well as the ionic conductivity, were found to be similar to those of the free bulk liquid, therefore suggesting the absence of solidification. Strong layering and a significant slowering of the IL dynamics, although without evidence of solidification, was observed in numerical simulations of ILs confined into a graphitic [75]. The same effect was also observed in a (rutile) titanium oxide nanoslit [76], with stronger effects in the rutile matrix, where stronger electrostatic and dispersion interactions are present between the individual ions of the IL and the pore wall, compared to the graphitic matrix.

Although the structuring of the ionic liquid into a solid nanoporous matrix has been so far investigated mostly by means of numerical simulations, it was recently revealed also experimentally. In Refs [77,78] the authors studied by small-angle X-ray scattering, NMR, and infrared spectroscopy ionogels formed by both hydrophilic [Bmim][BF$_4$] and hydrophobic [Hmim][PF$_6$] in a hydrophobic methylated silica matrix. A self-organized ordering of the IL was detected, with a better arrangement of ions in the matrix with a broader pore size distribution; this observation was explained by the authors by assuming that larger pores offer more room to the ions to accommodate the orientational disorder due to the internal pore roughness. The hydrophobic IL showed the closest packing inside the pores of the hydrophobic matrix.

The arrangement of imidazolium-based ILs in different silica matrices has been also studied by a combination of nitrogen sorption, mercury intrusion, and thermogravimetric analyses, as well as NMR spectroscopy [79], and neither significant layering nor solidification was observed.

Interfacial layering of bulk IL in contact with solid surfaces was reported by many authors, although it was not necessarily related to a structural liquid to solid-like transition. For example, layering was observed either by means of SFA [10] and AFM [33,80], including in the case of rough contacts [81]. Discrete interfacial layers whose separation is comparable to the diameter of the ions are interpreted as solvation layers, which are commonly observed in normal liquids in contact with a solid wall, including water [82]. The details of the solvation layers depend on the composition of the IL (anion and cation) and on the chemical properties of the substrate. In fact, the strong layering apparent in the case of mica progressively weakens in going to silica [33], graphite [33] and gold [83]. Layers are also observed by numerical simulations of IL thin films on solid surfaces, like on silica [84–86]. In molecular dynamics simulations, the limited duration of the simulation does not typically allow to observe equilibration into a solid-like phase in a sufficiently large system, if any. Interestingly, layering up to 9 nm has been detected via angle-resolved X-ray photoelectron spectroscopy in very thin imidazolium-based films deposited by evaporation in ultra-high vacuum on a gold surface

[40]. This is one of the very few examples of directly measured structural layering in thin films obtained by deposition of the pure liquid.

4. Ordering and solid-like properties of interfacial nanoconfined ILs

A robust experimental evidence of extended, highly packed layering in thin IL films, in some cases markedly solid-like in character, supported on metallic and insulating solid surfaces, have been collected in the last ten years [31,38,39,67,86–92]. The ordered structures typically extend in the direction perpendicular to the substrate by several nanometers, and in some cases tens of nanometers.

Jurado et al. recently observed an irreversible liquid to solid-like transition induced by squeezing [HMIM][EtSO$_4$] in a nanoscale gap between mica surfaces, using an extended SFA in dry N$_2$atmosphere [67]. The same results have been also obtained by the same authors using AFM equipped with 40 μm diameter colloidal silica probes. Discrete jumps in the force versus distance curves are observed, corresponding to breaking through solid-like IL layers (film-thickness transition). The number and the dimension of the fundamental transition layer increase upon successive approaches, up to an equilibrium condition. Figure 3(a) shows the reconstructed two-dimensional profile of the contact interface at maximum compression of the confined IL. Both force-separation curves acquired by eSFA (Figure 3(b)) and by AFM (Figure 3(c)) graphically describe the rupture events of successive film-transition layers, and the increase of the overall confined solid-like film thickness, during consecutive approaches. The observed mechanical response of the structured nanoconfined IL is qualitatively different from the one observed in solvation layer in bulk IL/
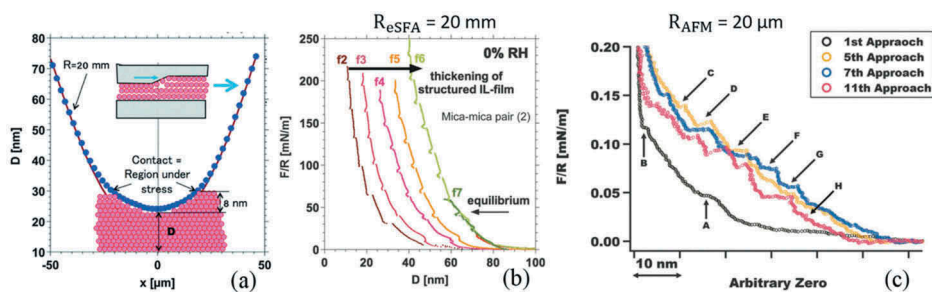
Figure 3. Irreversible liquid to solid transition induced by nanoconfinement of IL in the gap of an extended SFA, as reported in Ref [67]. (a) Measured 2D profile of the contact interface at maximum compression of the IL film. (b) Force – separation curves acquired by eSFA between mica surfaces across [Hmim] EtSO$_4$ in dry N$_2$ atmosphere during the 2nd to the 7th approaches (from left to right) at 1 nm s^{-1}. (c) Force–separation curves acquired by AFM for dry [Hmim] EtSO$_4$ on mica during the 1st, 5th, 7th, and 11th approaches in dry N$_2$ at constant speeds of 20 (1st approach) and 15 (subsequent approaches) nm s^{-1}. Adapted with permission from Ref [67].
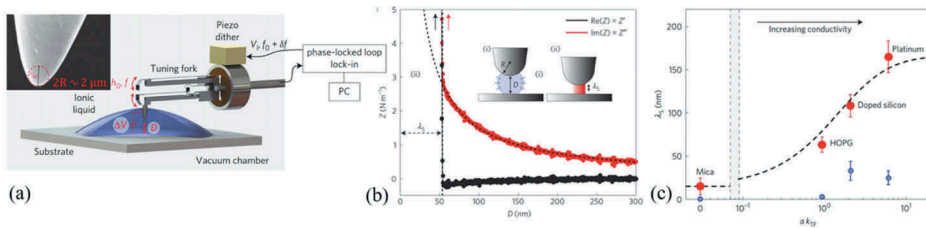
Figure 4. (a) Schematic representation of the tuning fork experiment and SEM image of typical tungsten tip. (b) Real (Z', black) and complex (Z'', red) part of the mechanical impedance as a function of the tungsten tip – HOPG surface distance. In the inset: scheme of the freezing induced by the confinement: upon a critical confinement length λ_S, the IL changes from liquid (i) to solid-like (ii). (c) Variation of the mean solidification length λ_S on mica and on three conductive substrates: HOPG, doped silicon, and platinum versus the normalized Thomas–Fermi wavevector, $a\,k$, with $2a$ being the typical ionic crystal lattice constant. Adapted with permission from Ref [31].

solid interfaces [80]. Interestingly, the same authors observed that water contamination prevents the liquid-to-solid transformation [93], which suggests that the presence of residual water can influence the behavior of the IL upon confinement.

Similar results have been obtained by Comtet et al. [31]. The authors used a tuning fork-based AFM equipped with a tungsten tip with radius up to 2.5 μm (shown in Figure 4(a)), and performed nanorheological measurements on [Bmim][BF4] on mica, HOPG, doped silicon, and platinum. While squeezing the film into the probe-surface nanoscale gap, the authors observed a dramatic change of the RTIL towards a solid-like phase, as soon as the separation, i.e. the squeezed film thickness, dropped below a threshold depending on the counter surface (HOPG, an example is shown in Figure 4(b)), in any case in the range 5–165 nm (as shown in Figure 4(c)). As discussed above, the authors interpreted their results in terms of a freezing transition, with the freezing–melting temperature that remarkably increased upon nanoconfinement, along with the observations of Jurado et al. [67].

Direct observations of solid-like ordering at room temperature of [Bmim] [NTf2] ionic liquid drop-casted on mica, amorphous silica, and oxidized silicon have been reported by the authors of this review in Refs [39,86,88,89]. Drop-casting consists in depositing on the substrate a small volume (few μl) of a highly diluted (typically 1 μg/ml) solution of IL in a suitable solvent; upon solvent evaporation, solid-like IL structures coexist with nano- and micrometer-sized liquid droplets of IL.

Solid-like structures have been observed on several insulating surfaces (mica, oxidized silicon, crystalline MgO, TiO_2, NaCl) using solvents with very different polarities (typically methanol, but also ethanol, and chloroform) (in Figure 5 a representative solid-like terrace formed on oxidized silicon is
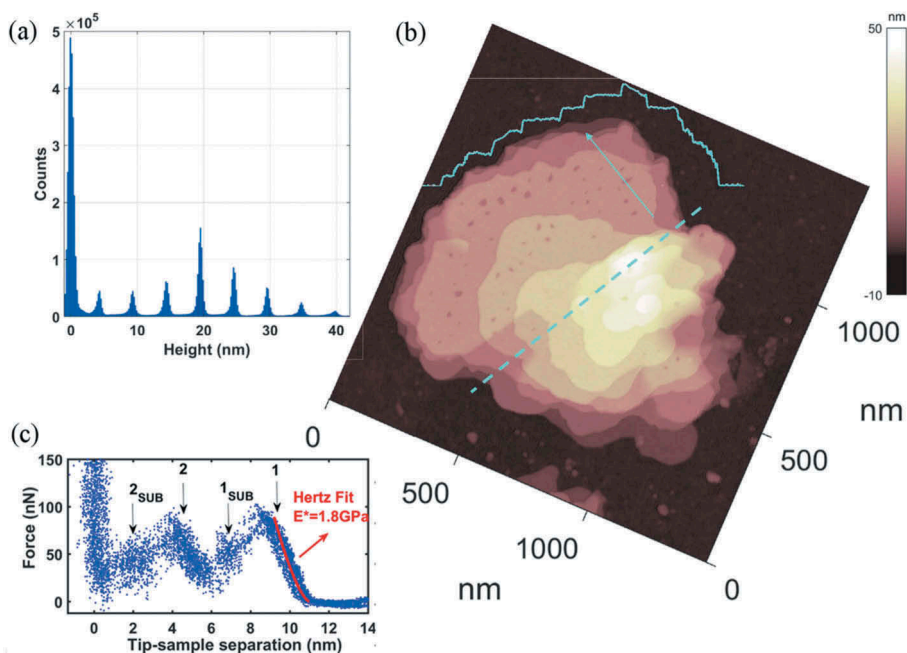
Figure 5. A solid-like [BMIM][NTf$_2$] layered structure (b) formed at room temperature upon deposition on an oxidized silicon surface of a microdroplet of a highly diluted (1 µg/ml) IL/methanol solution. The histogram of heights (a) shows that the thickness of each terrace is approximately 5 nm, each terrace composed of several molecular layers with height 0.6 nm [39]. The force versus indentation curves (c) reveal sequential penetration of solid-like stiff layers, with apparent Young's modulus of elasticity of approximately 1.8 GPa. Partially adapted with permission from Ref [88].

shown, with the corresponding height histogram). These ordered [Bmim][NTf2] structures are qualitatively different from the solvation layers [33,80], which are located in the first few interfacial layers of the bulk liquid in contact with a solid surface; the observed IL nanostructures are solid-like multi-layered micrometer-wide terraces, which extend from the surface up to several tens of nanometers. The terraces composing the observed structures are characterized by a perpendicular structural periodicity of ~0.6 nm, consistent with the ionic size of the IL, and in agreement with the results of numerical simulations of thin [Bmim][NTf2] layers on silica and mica [89,94]. Comparable thicknesses of the solid-like structures irreversibly formed upon nanoscale confinement under normal compressive stress were measured by Comtet et al. and by Jurado et al. using SFA and tuning-fork AFM [31,67].

Experimental evidences discussed in the cited works suggest that these [Bmim][NTf$_2$] structures formed by drop-casting on oxidized silicon and other insulating smooth substrates are not only vertically ordered but also possess a mechanical resistance to compressive stresses that are typical of solid materials, with a measured Young's modulus of a few GPa [88,89].
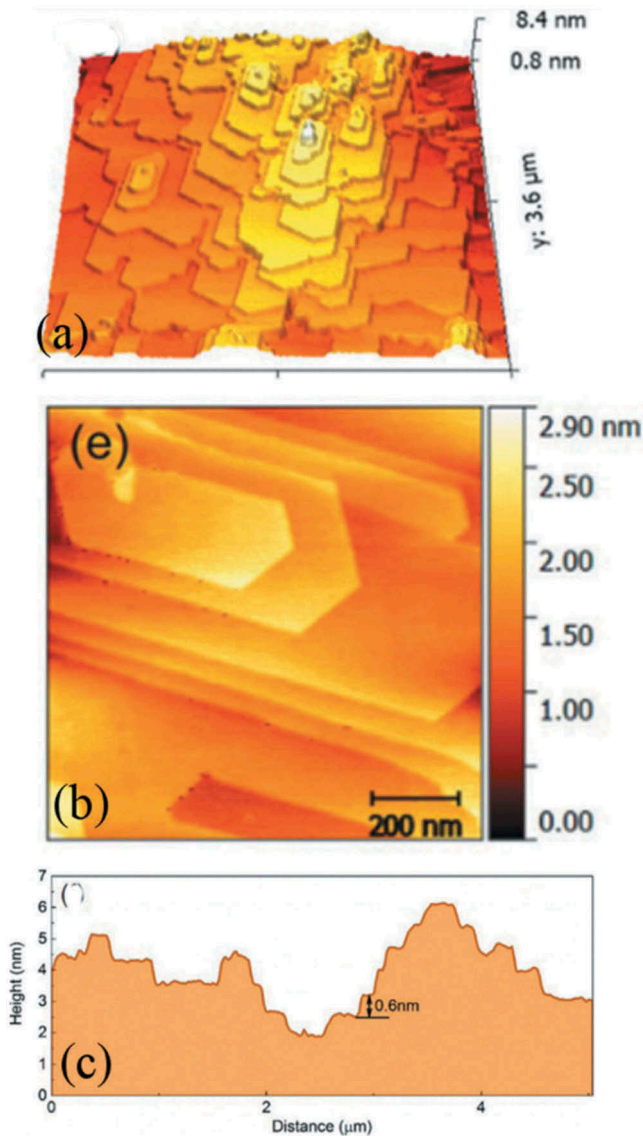
Figure 6. (a) Large-scale and (b) higher-resolution AFM topographic images of [Bmim][NTFI] intercalated in the mica. (c) A representative stepped profile section of an IL nanostructure intercalated in the mica. Adapted with permission from Ref [68].

Beyond a critical pressure of the order of 1 GPa, the AFM tip sequentially penetrates several solid-like terraces (Figure 5). In conditions of strong surface interaction and nanoscale confinement, these rigid structures are also highly resilient to intense electric fields, and possess an electrically insulating character, with a dielectric constant ε_r between 3 and 5, similar to that of conventional solid salts [88].

A recent interesting work reports the formation of highly ordered [Bmim] [NTFI] structures under confinement upon intercalation in between mica sheets [68]. The structures formed upon intercalation and consequent nano-confinement were revealed by stripping the topmost mica sheets and directly imaged by AFM (Figure 6(a,b)). These structures appear like crystals (also probed by X-ray diffraction) stacked into well-defined regular terraces with fundamental height of 0.6 nm (Figure 6(c)) and width of several microns. The dimension of the fundamental terrace step confirms the results obtained in Ref [86], and is consistent with the ionic size of [Bmim][NTFI].

Differential scanning calorimetry showed that once the layered structures are developed, they remain stable until melting at a temperature, which is 73 K higher than that of the corresponding bulk IL. This reminds us of the increase of the melting point of ILs upon confinement observed by other authors, as discussed before [31]. Furthermore, the crystallized ILs exhibit very regular geometrical shapes, following the hexagonal symmetry of the mica surface, indicating an epitaxial relation between IL and mica, which acts here as a template.

We notice here that squeezing an IL layer between two surfaces, depositing an IL thin film by drop-casting from an IL-methanol solution or depositing IL on an intercalating lamellar solid-like mica, share some characters that may be very relevant for the formation of ordered, layered, solid-like structures.

Firstly, in all these cases there is strong confinement of the IL, and the region occupied by the IL has high surface to volume ratio, at odd with the cases where a bulk amount of IL is deposited onto a solid surface. Physical vapor deposition of IL in ultra-high vacuum is another strategy to deposit ILs in such confined, strongly surface interacting condition [40]. Similarly, the deposition of nanoliters of pure IL on a surface by ink-jet printing is another way of producing a strongly confined interfacial IL system [92]. Not surprisingly, also in the case of Ref [40], strong layering of pure IL in the thin film regime is observed (while in the case of Ref [92] layering was speculated, but unfortunately not directly tested). In the case of drop-casting onto solid surfaces of highly diluted IL – volatile solvent solutions, the condition of strong interfacial interaction is favored by the sequential fragmentation of the evaporating liquid film into smaller and smaller droplets, containing small amounts of IL. Liquid to solid-like transition of the IL likely takes place whenever the amount of IL entrapped in the small evaporating droplet is below a critical threshold, where energetically the transition is favored with respect to the IL remaining in the liquid phase. The randomness of the dewetting process of the evaporating liquid film in drop-casting deposition leads to the observed coexistence of liquid and solid-like IL domains.
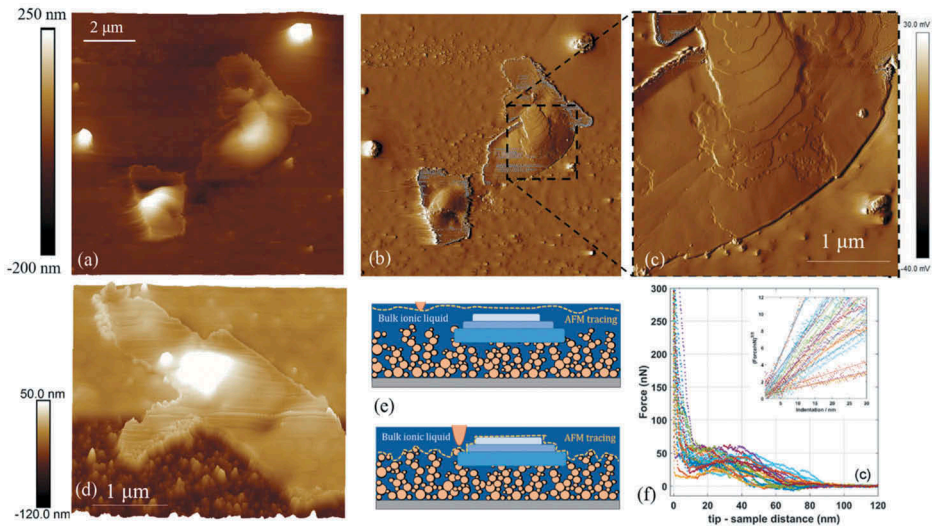
Figure 7. AFM morphological (a,d) and amplitude error (b,c) maps of a ns-SiOx surface after deposition of 5 µl of 0.5:1000 [Bmim][NTf2]/methanol solution onto the nanostructured surface. (e) Schematic representation of the scanning principle of AFM in the upper and lower part of figure (d). (f) Indentation curves acquired on the structured solid-like terrace of Figure (d). Partially adapted with permission from Ref [87].

Secondly, in all the experiments described so far, there is an external driving force favoring the ordered arrangement of the ions. In the case of the force versus distance experiments with large contact areas, the driving force is the normal compressive stress. In drop-casting deposition, the driving force is probably provided by convection inside the evaporating solvent droplet, where also density and temperature gradients are present; energetically, the endothermic evaporation of the solvent may also play a role, that should be better quantified. In the case of intercalation of IL into mica sheets, the extreme confinement conditions like those encountered into nanoporous materials are satisfied. These favorable interactions met by the IL in the described experimental conditions can drive the crystallization, or formation of an ordered solid-like phase, overcoming kinetic barriers, pinning due to contaminants and local defects of the host matrix, etc.

The above discussion on the formation of solid-like nanostructures of ILs upon confinement in open geometries can help understanding the phenomenology of interfacial ordering at rough, nanostructured surfaces. These interfaces are paradigmatic of ionogels used in devices employing IL as electrolytes and nanostructured, nanoporous materials as electrodes.

In Ref [87] we recently reported the results of a systematic characterization, performed by AFM, of the morphological and mechanical properties of [Bmim][NTf$_2$] thin films supported on a rough nanostructured oxidized silicon surface produced by SCBD.

We observed that the high roughness and nanoscale porosity of the oxidized silicon film did not prevent the formation of solid-like IL domains, even when they are surrounded by the IL in the liquid phase (Figure 7). The solid-like [Bmim][NTf$_2$] terraces coexist with the liquid phase. At higher IL concentrations, the solid-like structures are typically embedded in a liquid film with thickness up to several nanometers, without this causing disruption of the slid-like order.

Furthermore, the Young's modulus of the solid-like structures was measured by AFM indentation (Figure 7(f)) and confirmed to be on the tens of MPa range, comparable to that of relatively stiff plastics, although significantly smaller than that of similar structures formed on smooth silica substrates (up to a few GPa) [88]. Similarly, to the structures formed on smooth substrates [88], also those formed on nanostructured SiOx seems to possess an insulating character, according to their charging behavior under exposure to electron beams (see the Supporting Information of Ref [88]).

The experimental results reported in this last section about the interfacial ordering of ILs upon nanoscale confinement highlight the liquid-solid transition of supported ILs on nanostructured and porous materials, as suggested and supported by the observations of the increase of the melting point and by the other recent experimental and numerical findings discussed in this review.

5. Conclusions

The study of the physical properties of ILs in strongly confined geometries, and in particular into nanoporous materials, is still in its infancy, despite the intense efforts of several research groups and its great importance for the applications.

Significant changes in the structural and physical properties of ILs confined into nanoporous matrices have been reported, which could strongly affect the behavior of devices employing ionogels. In particular, ILs in strong confinement conditions can undergo a liquid to solid-like transition, which dramatically affects their physical properties like the ionic mobility, the viscosity, and the electrical properties. However, a clear picture is still missing, and controversial reports can be found in the literature. The diversity of results and also the discrepancies in the behavior of nanoconfined ILs reported in the literature, and partially discussed in this review, can be attributed to several factors: (i) the still unclear role of impurities, such as water; (ii) the specific nature of cation and anion; (iii) the wetting behavior of the IL with respect to the solid walls of the matrix; (iv) the details of the confining matrix, (v) other interfacial or molecular properties. Controlling or even simply characterizing these diverse properties by means of theoretical modeling, numerical simulations and experiments is a challenge.

In particular, when studying ionogels, one has to consider also the importance of producing host matrices with controlled nanostructure and chemical properties, which in turn points to the need of developing reliable synthetic methods. Here we have shown that cluster-assembling of nanostructured thin electrodes and atomic force microscopy represent a versatile and powerful tool to address the many open questions. Nevertheless, while the investigation of open interfacial geometries will likely progress significantly in the next future thanks to the existing methodologies, a greater effort will be required to study the behavior of ILs into the bulk of the nanoporous host matrices, which is not directly accessible to AFM or several other surface characterization techniques.

Acknowledgments

Disclosure Statement

No potential conflict of interest was reported by the authors.

ORCID

Francesca Borghi http://orcid.org/0000-0001-6980-4910
Alessandro Podestà http://orcid.org/0000-0002-4169-6679

References

[1] Hallett JP, Welton T. Room-temperature ionic liquids: solvents for synthesis and catalysis. 2. Chem Rev. 2011;111:3508–3576.
[2] Welton T. Room-temperature ionic liquids. Solvents for synthesis and catalysis. Chem Rev. 1999;99:2071–2084.
[3] Ohno H, editor. Electrochemical aspects of ionic liquids. 2nd ed. Hoboken, NJ: Wiley; 2011.
[4] Bermúdez M-D, Jiménez A-E, Sanes J, et al. Ionic liquids as advanced lubricant fluids. Molecules. 2009;14:2888–2908.
[5] Palacio M, Bhushan B. A review of ionic liquids for green molecular lubrication in nanotechnology. Tribol Lett. 2010;40:247–268.
[6] Xiao H. Ionic liquid lubricants: basics and applications. Tribol Trans. 2017;60:20–30.
[7] Zhou F, Liang Y, Liu W. Ionic liquid lubricants: designed chemistry for engineering applications. Chem Soc Rev. 2009;38:2590–2599.
[8] Plechkova NV, Seddon KR. Applications of ionic liquids in the chemical industry. Chem Soc Rev. 2007;37:123–150.

[9] Galiński M, Lewandowski A, Stępniak I. Ionic liquids as electrolytes. Electrochim Acta. 2006;51:5567–5580.

[10] Perkin S. Ionic liquids in confined geometries. Phys Chem Chem Phys. 2012;14:5052.

[11] Balducci A, Soavi F, Mastragostino M. The use of ionic liquids as solvent-free green electrolytes for hybrid supercapacitors. Appl Phys A. 2006;82:627–632.

[12] Bettini LG, Piseri P, De Giorgio F, et al. Flexible, ionic liquid-based micro-supercapacitor produced by supersonic cluster beam deposition. Electrochim Acta. 2015;170:57–62.

[13] Bettini LG, Galluzzi M, Podestà A, et al. Planar thin film supercapacitor based on cluster-assembled nanostructured carbon and ionic liquid electrolyte. Carbon. 2013;59:212–220.

[14] Lau GPS, Décoppet J-D, Moehl T, et al. Robust high-performance dye-sensitized solar cells based on ionic liquid-sulfolane composite electrolytes. Sci Rep. 2016;5:18158.

[15] Zhao Y, Bostrom T. Application of ionic liquids in solar cells and batteries: a review. Curr Org Chem. 2015;19:556–566.

[16] Lewandowski A, Świderska-Mocek A. Ionic liquids as electrolytes for Li-ion batteries—an overview of electrochemical studies. J Power Sources. 2009;194:601–609.

[17] Navarra MA. Ionic liquids as safe electrolyte components for Li-metal and Li-ion batteries. MRS Bull. 2013;38:548–553.

[18] Zhang S, Zhang J, Zhang Y, et al. Nanoconfined ionic liquids. Chem Rev. 2017;117:6755–6833.

[19] Zhang S, Dokko K, Watanabe M. Porous ionic liquids: synthesis and application. Chem Sci. 2015;6:3684–3691.

[20] Singh MP, Singh RK, Chandra S. Ionic liquids confined in porous matrices: physico-chemical properties and applications. Pro Mater Sci. 2014;64:73–120.

[21] Dai S, Ju YH, Gao HJ, et al. Preparation of silica aerogel using ionic liquids as solvents. Chem Commun. 2000;3:243–244.

[22] Simon P, Gogotsi Y. Materials for electrochemical capacitors. Nat Mater. 2008;7:845–854.

[23] Armand M, Endres F, MacFarlane DR, et al. Ionic-liquid materials for the electro-chemical challenges of the future. Nat Mater. 2009;8:621–629.

[24] Merlet C, Rotenberg B, Madden PA, et al. On the molecular origin of supercapaci-tance in nanoporous carbon electrodes. Nat Mater. 2012;11:306–310.

[25] Trewyn BG, Whitman CM, Lin VS-Y. Morphological control of room-temperature ionic liquid templated mesoporous silica nanoparticles for controlled release of antibacterial agents. Nano Lett. 2004;4:2139–2143.

[26] Selvam T, Machoke A, Schwieger W. Supported ionic liquids on non-porous and porous inorganic materials—a topical review. Appl Catal A Gen. 2012;445–446:92–101.

[27] Van Doorslaer C, Wahlen J, Mertens P, et al. Immobilization of molecular catalysts in supported ionic liquid phases. Dalton Trans. 2010;39:8377.

[28] Romanos GE, Stefanopoulos KL, Vangeli OC, et al. Investigation of physically and chemically ionic liquid confinement in nanoporous materials by a combination of SANS, contrast-matching SANS, XRD and nitrogen adsorption. J Phys Conf Ser. 2012;340:012087.

[29] Chen S, Wu G, Sha M, et al. Transition of ionic liquid [bmim][PF6] from liquid to high-melting-point crystal when confined in multiwalled carbon nanotubes. J Am Chem Soc. 2007;129:2416–2417.

[30] Im J, Cho SD, Kim MH, et al. Anomalous thermal transition and crystallization of ionic liquids confined in graphene multilayers. Chem Commun. 2012;48:2015–2017.

[31] Comtet J, Niguès A, Kaiser V, et al. Nanoscale capillary freezing of ionic liquids confined between metallic interfaces and the role of electronic screening. Nat Mater. 2017;16:634–639.

[32] An R, Zhu Y, Wu N, et al. Wetting behavior of ionic liquid on mesoporous titanium dioxide surface by atomic force microscopy. ACS Appl Mater Interfaces. 2013;5:2692–2698.

[33] Atkin R, Warr GG. Structure in confined room-temperature ionic liquids. J Phys Chem C. 2007;111:5162–5168.

[34] Wakeham D, Hayes R, Warr GG, et al. Influence of temperature and molecular structure on ionic liquid solvation layers. J Phys Chem B. 2009;113:5961–5966.

[35] Chathoth SM, Mamontov E, Dai S, et al. Fast diffusion in a room temperature ionic liquid confined in mesoporous carbon. EPL. 2012;97:66004.

[36] Iacob C, Sangoro JR, Papadopoulos P, et al. Charge transport and diffusion of ionic liquids in nanoporous silica membranes. Phys Chem Chem Phys. 2010;12:13798–13803.

[37] Hazelbaker ED, Guillet-Nicolas R, Thommes M, et al. Influence of confinement in mesoporous silica on diffusion of a mixture of carbon dioxide and an imidazolium-based ionic liquid by high field diffusion NMR. Microporous Mesoporous Mater. 2015;206:177–183.

[38] Liu Y, Zhang Y, Wu G, et al. Coexistence of liquid and solid phases of Bmim-PF$_6$ ionic liquid on mica surfaces at room temperature. J Am Chem Soc. 2006;128:7456–7457.

[39] Bovio S, Podestà A, Lenardi C, et al. Evidence of extended solidlike layering in [Bmim][NTf2] ionic liquid thin films at room-temperature. J Phys Chem B. 2009;113:6600–6603.

[40] Cremer T, Killian M, Gottfried JM, et al. Physical vapor deposition of [EMIM][Tf$_2$N]: a new approach to the modification of surface properties with ultrathin ionic liquid films. Chem Phys Chem. 2008;9:2185–2190.

[41] Wegner K, Piseri P, Tafreshi HV, et al. Cluster beam deposition: a tool for nanoscale science and technology. J Phys D Appl Phys. 2006;39:R439–R459.

[42] Bideau JL, Viau L, Vioux A. Ionogels, ionic liquid based hybrid materials. Chem Soc Rev. 2011;40:907–925.

[43] Viau L, Tourné-Péteilh C, Devoisselle J-M, et al. Ionogels as drug delivery system: one-step sol–gel synthesis using imidazolium ibuprofenate ionic liquid. Chem Commun. 2009;46:228–230.

[44] Nanoporous carbon supercapacitors in an ionic liquid: a computer simulation study. Available from: https://pubs.acs.org/doi/abs/10.1021/nn901916m.

[45] Sheberla D, Bachman JC, Elias JS, et al. Conductive MOF electrodes for stable supercapacitors with high areal capacitance. Nat Mater. 2017;16:220–224.

[46] Fujie K, Otsubo K, Ikeda R, et al. Low temperature ionic conductor: ionic liquid incorporated within a metal–organic framework. Chem Sci. 2015;6:4306–4310.

[47] Parsons R. The electrical double layer: recent experimental and theoretical developments. Chem Rev. 1990;90:813–826.

[48] Pandolfo AG, Hollenkamp AF. Carbon properties and their role in supercapacitors. J Power Sources. 2006;157:11–27.

[49] Xu W, Angell CA. Solvent-free electrolytes with aqueous solution-like conductivities. Science. 2003;302:422–425.

[50] Chmiola J, Yushin G, Gogotsi Y, et al. Anomalous increase in carbon capacitance at pore sizes less than 1 nanometer. Science. 2006;313:1760–1763.

[51] Raymundo-Piñero E, Kierzek K, Machnikowski J, et al. Relationship between the nanoporous texture of activated carbons and their capacitance properties in different electrolytes. Carbon. 2006;44:2498–2507.

[52] Sayago J, Meng X, Quenneville F, et al. Electrolyte-gated polymer thin film transistors making use of ionic liquids and ionic liquid-solvent mixtures. J Appl Phys. 2015;117:112809.

[53] Barborini E, Piseri P, Milani P. A pulsed microplasma source of high intensity supersonic carbon cluster beams. J Phys D: Appl Phys. 1999;32:L105.

[54] Borghi F, Milani M, Bettini LG, et al. Quantitative characterization of the interfacial morphology and bulk porosity of nanoporous cluster-assembled carbon thin films. Appl Surf Sci. 2019;479:395–402.

[55] Soavi F, Bettini LG, Piseri P, et al. Miniaturized supercapacitors: key materials and structures towards autonomous and sustainable devices and systems. J Power Sources. 2016;326:717–725.

[56] Podestà A, Borghi F, Indrieri M, et al. Nanomanufacturing of titania interfaces with controlled structural and functional properties by supersonic cluster beam deposition. J Appl Phys. 2015;118:234309.

[57] Borghi F, Podestà A, Di Vece M, et al. Cluster-assembled materials: from fabrication to function, in encyclopedia of interfacial chemistry: surface science and electrochemistry. Wandelt Klaus. 2018:417–427.

[58] Borghi F, Podestà A, Piazzoni C, et al. Growth mechanism of cluster-assembled surfaces: from submonolayer to thin-film regime. Phys Rev Appl. 2018;9:044016.

[59] Borghi F, Sogne E, Lenardi C, et al. Cluster-assembled cubic zirconia films with tunable and stable nanoscale morphology against thermal annealing. J Appl Phys. 2016;120:055302.

[60] Bongiorno G, Podesta A, Ravagnan L, et al. Electronic properties and applications of cluster-assembled carbon films. J Mater Sci. 2006;17:427–441.

[61] Yi Z, Bettini LG, Tomasello G, et al. Flexible conducting polymer transistors with supercapacitor function. J Polym Sci Part B Polym Phys. 2017;55:96–103.

[62] Tripathi AK, Verma YL, Singh RK. Thermal, electrical and structural studies on ionic liquid confined in ordered mesoporous MCM-41. J Mater Chem A. 2015;3:23809–23820.

[63] Kanakubo M, Hiejima Y, Minami K, et al. Melting point depression of ionic liquids confined in nanospaces. Chem Commun. 2006;17:1828–1830.

[64] Alba-Simionesco C, Coasne B, Dosseh G, et al. Effects of confinement on freezing and melting. J Phys. 2006;18:R15–R68.

[65] Knight AW, Kalugin NG, Coker E, et al. Water properties under nano-scale confinement. Sci Rep. 2019;9:8246.

[66] Klein J, Kumacheva E. Simple liquids confined to molecularly thin layers. I. Confinement-induced liquid-to-solid phase transitions. J Chem Phys. 1998;108:6996–7009.

[67] Jurado LA, Kim H, Arcifa A, et al. Irreversible structural change of a dry ionic liquid under nanoconfinement. Phys Chem Chem Phys. 2015;17:13613–13624.

[68] Lu Y, Chen W, Wang Y, et al. Space-confined strategy toward large-area two-dimensional crystals of ionic liquid. Phys Chem Chem Phys. 2019;22:1820–1825.

[69] Tripathi AK, Singh RK. Immobilization induced molecular compression of ionic liquid in ordered mesoporous matrix. J Phys D Appl Phys. 2018;51:075301.

[70] Neouze M-A, Litschauer M. Confinement of 1-Butyl-3-methylimidazolium nitrate in metallic silver. J Phys Chem A. 2008;112:16721–16725.

[71] Fujie K, Yamada T, Ikeda R, et al. Introduction of an ionic liquid into the micropores of a metal–organic framework and its anomalous phase behavior. Angew Chem. 2014;53:11302–11305.

[72] Marion S, Davis SJ, Wu Z-Q, et al. Nanocapillary confinement of imidazolium based ionic liquids. *arXiv:1909.05234 [cond-mat, physics: physics]*. 2019.

[73] Waechtler M, Sellin M, Stark A, et al. 2H and 19F solid-state NMR studies of the ionic liquid [C2Py][BTA]-d10 confined in mesoporous silica materials. Phys Chem Chem Phys. 2010;12:11371.

[74] Ori G, Villemot F, Viau L, et al. Ionic liquid confined in silica nanopores: molecular dynamics in the isobaric–isothermal ensemble. Mol Phys. 2014;112:1350–1361.

[75] Rajput NN, Monk J, Hung FR. Structure and dynamics of an ionic liquid confined inside a charged slit graphitic nanopore. J Phys Chem C. 2012;116:14504–14513.

[76] Singh R, Rajput NN, He X, et al. Molecular dynamics simulations of the ionic liquid [EMIM+][TFMSI−] confined inside rutile (110) slit nanopores. Phys Chem Chem Phys. 2013;15:16090.

[77] Wu C-M, Lin S-Y, Kao K-Y, et al. Self-organization of a hydrophilic short-chain ionic liquid confined within a hydrophobic nanopore. J Phys Chem C. 2014;118:17764–17772.

[78] Wu C-M, Lin S-Y. Close packing existence of short-chain ionic liquid confined in the nanopore of silica ionogel. J Phys Chem C. 2015;119:12335–12344.

[79] Heinze MT, Zill JC, Matysik J, et al. Solid–ionic liquid interfaces: pore filling revisited. Phys Chem Chem Phys. 2014;16:24359–24372.

[80] Hayes R, Warr GG, Atkin R. At the interface: solvation and designing ionic liquids. Phys Chem Chem Phys. 2010;12:1709.

[81] Sheehan A, Jurado LA, Ramakrishna SN, et al. Layering of ionic liquids on rough surfaces. Nanoscale. 2016;8:4094–4106.

[82] Israelachvili JN, Pashley RM. Molecular layering of water at surfaces and origin of repulsive hydration forces. Nature. 1983;306:249–250.

[83] Atkin R, El Abedin SZ, Hayes R, et al. AFM and STM Studies on the Surface Interaction of [BMP]TFSA and [EMIm]TFSA Ionic Liquids with Au(111). J Phys Chem C. 2009;113:13266–13272.

[84] Shimizu K, Pensado A, Malfreyt P, et al. 2D or not 2D: structural and charge ordering at the solid-liquid interface of the 1-(2-hydroxyethyl)-3-methylimidazolium tetrafluoroborate ionic liquid. Faraday Discuss. 2012;154:155–169.

[85] Mendonça ACF, Malfreyt P, Pádua AAH. Interactions and ordering of ionic liquids at a metal surface. J Chem Theory Comput. 2012;8:3348–3355.

[86] Bovio S, Podestà A, Milani P, et al. Nanometric ionic-liquid films on silica: a joint experimental and computational study. J Phys Condens Matter. 2009;21:424118.

[87] Borghi F, Milani P, Podestà A. Solid-like ordering of imidazolium-based ionic liquids at rough nanostructured oxidized silicon surfaces. Langmuir. 2019;35:11881–11890.

[88] Galluzzi M, Bovio S, Milani P, et al. Surface confinement induces the formation of solid-like insulating ionic liquid nanostructures. J Phys Chem C. 2018;122:7934–7944.

[89] Ballone P, Pópolo MGD, Bovio S, et al. Nano-indentation of a room-temperature ionic liquid film on silica: a computational experiment. Phys Chem Chem Phys. 2012;14:2475–2482.

[90] Gong X, Kozbial A, Li L. What causes extended layering of ionic liquids on the mica surface? Chem Sci. 2015;6:3478–3482.

[91] Fukui K, Yokota Y, Imanishi A. Local analyses of ionic liquid/solid interfaces by frequency modulation atomic force microscopy and photoemission spectroscopy: analysis of ionic liquid/solid interfaces. Chem Rec. 2014;14:964–973.

[92] Kaisei K, Kobayashi K, Matsushige K, et al. Fabrication of ionic liquid thin film by nano-inkjet printing method using atomic force microscope cantilever tip. Ultramicroscopy. 2010;110:733–736.

[93] Jurado LA, Kim H, Rossi A, et al. Effect of the environmental humidity on the bulk, interfacial and nanoconfined properties of an ionic liquid. Phys Chem Chem Phys. 2016;18:22719–22730.

[94] Dragoni D, Manini N, Ballone P. Interfacial layering of a room-temperature ionic liquid thin film on mica: a computational investigation. Chem Phys Chem. 2012;13:1772–1780.